



A structure/function study of polyamidoamine dendrimer as a steel corrosion inhibitor

K.F. Khaled^{1,2*}, A. A. Atta^{3,4}, N. S. Abdel-Shafi^{2,5}

¹Materials and Corrosion Laboratory, Chemistry Department, Faculty of Science, Taif University, Saudi Arabia

²Electrochemistry Research Laboratory, Chemistry Department, Faculty of Education, Ain Shams Univ., Roxy, Cairo, Egypt

³Physics Department, Faculty of Science, Ain Taif University, Saudi Arabia

⁴Physics Department, Faculty of Education, Ain Shams University, Roxy, 11757 Cairo, Egypt

⁵Chemistry Department, Faculty of Science, Hail University, Saudi Arabia

Received 20 Nov 2013, Revised 08 Feb. 2014, Accepted 09 Feb. 2014

*Corresponding Author. E-mail: k.khaled@tu.edu.sa; Tel: (+966550670425)

Abstract

A novel application of dendrimer technology is described in the present paper that use dendrimer molecule as a corrosion inhibitor for steel in molar hydrochloric acid. Inhibition effectiveness of polyamidoamine dendrimer (PAMAM) was assessed through potentiodynamic polarization and electrochemical impedance spectroscopy measurements. Polarization curves show that PAMAM acts as cathodic-type inhibitor. Electrochemical impedance spectroscopy, EIS plots shows that addition of PAMAM increases the polarization resistance of the corrosion process, and hence the inhibition efficiency. The molecular dynamics simulation results show that PAMAM can adsorb on the steel surface through the nitrogen atoms as well as π -electrons in the dendrimer structure.

Keywords: Steel; EIS; Polarization; Modeling studies; Corrosion

1. Introduction

Steel finds wide application in a broad field of industry and machinery. However its tendency to corrode makes it unsuitable for exposure to acids. For example, the scale formation in steel boilers is a quite common problem in industries which has to be removed. Hydrochloric acid is used for removing scales from the boiler surface. To minimize the steel loss during this process, corrosion inhibition programs are required. The corrosion inhibition is achieved by the addition of inhibitor to the system that prevents corrosion of the metal surface. The influence of the inhibitor upon steel corrosion is often associated with physical or chemical adsorption [1, 2].

At present, most of the inhibitors are small molecular organic compounds containing hetero-atoms, such as nitrogen, oxygen, sulphur and phosphor [3-21]. Relying on the actions of these hetero-atoms, inhibitors are adsorbed onto the metal surface, and block the metal surface and thus do not permit the corrosion process to take place[3].

The long chain carbon linkage and multiple adsorption sites of the polymers can block large area of the corroding metal[22]. The adsorbed film on the metal surface acts as a barrier isolating the metal from the aggressive anions present in solution. Cost, health issues, and environmental regulation restrictions have made researchers focus on the development of non-toxic polymers used as corrosion inhibitors[22].

The most popular class of highly branched molecules, dendrimers, has been intensively studied for two decades. A lot of exciting results related to chemical architectures, synthetic routines, encapsulating properties, aggregation behaviour, assembly in solution and surfaces in conjunction with prospective applications in drug delivery, nano-composite materials, and catalytic systems have been reported [11, 23-27]

Dendrimers are highly symmetrical macromolecules of nanometre scale consisting of branching units attached to a central poly-functional core[28]. They have a perfectly branched structure with radial symmetry and a unique molecular weight. The number of self-similar synthesis steps is referred to as generation of the dendrimer. Dendrimers have attracted immense attention during the last decade due to their interesting properties both from a basic and an applied research viewpoint. They show a low viscosity in solution and have a high shape stability, despite being a molecule of large molecular weight[28]. Encapsulation of metal

numerical with polarization (DNP) basis set, since this was the best set available in DMol³. All computations were performed with spin polarization.

The phenomenon of electrochemical corrosion takes place in the water phase, so it is relevant to include the effect of solvent in the computations. Self-consistent reaction field (SCRF) theory, with Tomasi's polarised continuum model (PCM) will be used to perform the calculations in solution. These methods model the solvent as a continuum of uniform dielectric constant ($\epsilon=78.5$) and define the cavity where the solute is placed as a uniform series of interlocking atomic spheres. Frontier orbital distribution will obtain, at the same basis set level, to analyze the reactivity of inhibitor molecules.

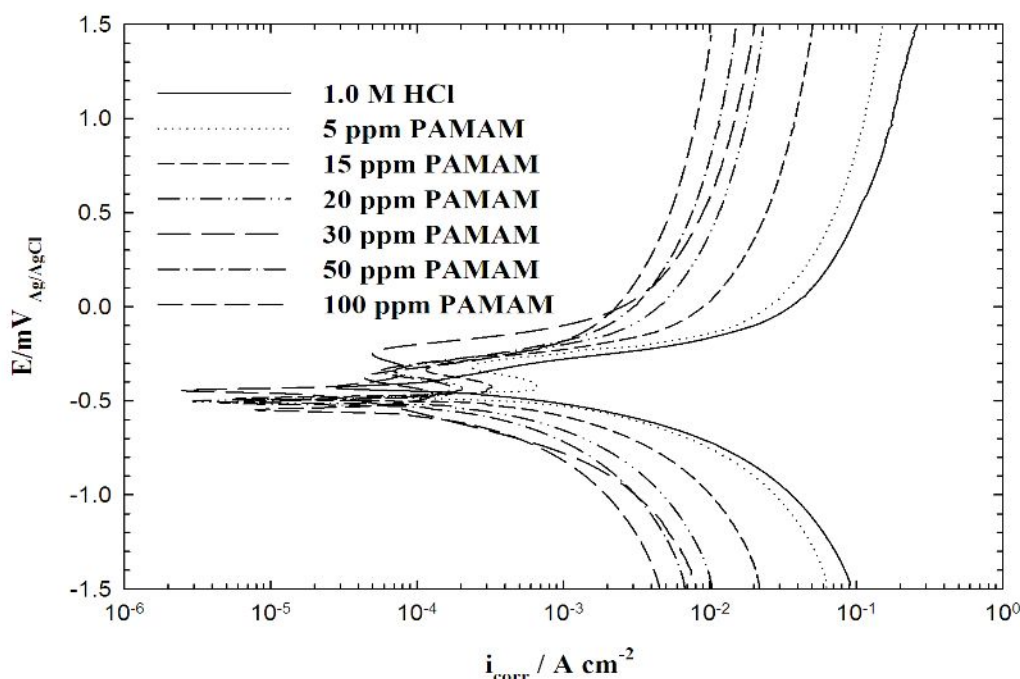


Figure 2: Anodic and cathodic potentiodynamic polarization curves for steel 5LX60 in 1.0 M HCl solutions in absence and presence of various concentrations of polyamidoamine dendrimer at 25 ± 1 °C.

In this study, a modeling scheme aimed at determination of the interactions between (PAMAM) and the steel surface. The modelling procedure is similar to methods used to predict polymer miscibility and phase behavior. The steps in this modeling scheme are outlined below:

- Generate models of the (PAMAM)dendrimer using geometry optimization technique.
- Generate models of the iron (111) substrate.
- Generate several hundred pair configurations by choosing random values for the six spatial variables that describe the relative orientations of two objects.
- Optimize the atomic coordinates of the model by minimizing the molecular potential energy of the system. The coordinates of the inorganic surface were fixed at their ideal crystalline positions.
- Compute the pair interaction energy for each configuration.
- Identify the lowest energy configuration.
- Generate a 1 picosecond trajectory at 300 degrees C using a molecular dynamics method starting from the lowest energy configuration.
- Report the average polymer-surface interaction energy obtained during the molecular dynamics simulation.

4. Results and discussions

4.1 Electrochemical investigation

Figure 2 represents the potentiodynamic polarization curves obtained on steel in 1.0 M HCl solution without and with addition of (PAMAM) dendrimer. In all cases, addition of different concentrations of PAMAM induces significant decrease in both anodic and cathodic currents. The observed decrease in cathodic currents was the greatest at concentration of 100 ppm.

Table 1: Electrochemical parameters calculated from polarization measurements on steel 5LX60 electrode in 1M HCl solutions without and with various concentrations of polyamidoamine dendrimer at 25 ±1 °C by potentiodynamic polarization measurements.

| Conc. ppm | I_{corr} $\mu A.cm^{-2}$ | $-E_{corr}$ mV | b_a $mV.dec^{-1}$ | $-b_c$ $mV.dec^{-1}$ | C.R mpy | E_T % |
|-----------|----------------------------|----------------|---------------------|----------------------|---------|---------|
| 0.00 | 238 | 426 | 207.7 | 233.1 | 108.8 | ----- |
| 5 | 121 | 448 | 208.1 | 317 | 55.32 | 49.16 |
| 15 | 81.1 | 470 | 246 | 284 | 37.06 | 65.93 |
| 20 | 63.4 | 493 | 268 | 334 | 28.98 | 73.36 |
| 30 | 56.5 | 498 | 279 | 328 | 25.1 | 76.26 |
| 50 | 43.5 | 501 | 260 | 332 | 19.85 | 81.72 |
| 100 | 26.7 | 517 | 307 | 341 | 12.21 | 88.78 |

The increase in PAMAM concentration shifts E_{corr} cathodically, lowers the cathodic current densities with simultaneous increase in Tafel constant b_c and b_a .

Electrochemical parameters E_{corr} and Tafel slopes determined from the polarization curves in Figure 2 are listed in Table 1. The values of corrosion currents determined by the extrapolation of Tafel curves to E_{corr} are also presented in Table 1 together with the inhibitor efficiency E_T %, which was calculated from potentiodynamic polarization measurements using the following equation [42]:

$$E_T \% = \left(1 - \frac{i_{corr}}{i_{corr}^0}\right) \times 100 \quad (1)$$

where i_{corr}^0 and i_{corr} correspond to uninhibited and inhibited current densities, respectively.

The polarization measurements show, in all cases, that addition of the inhibitor induces a decrease in both cathodic and anodic currents with a negative shift of corrosion potential and accordingly, PAMAM acts as a cathodic type inhibitor.

The results of the EIS measurements were presented in Figures 3-5 as Nyquist and Bode plots. Impedance measurements were conducted in 1.0 M HCl solutions without and with different concentrations of the PAMAM.

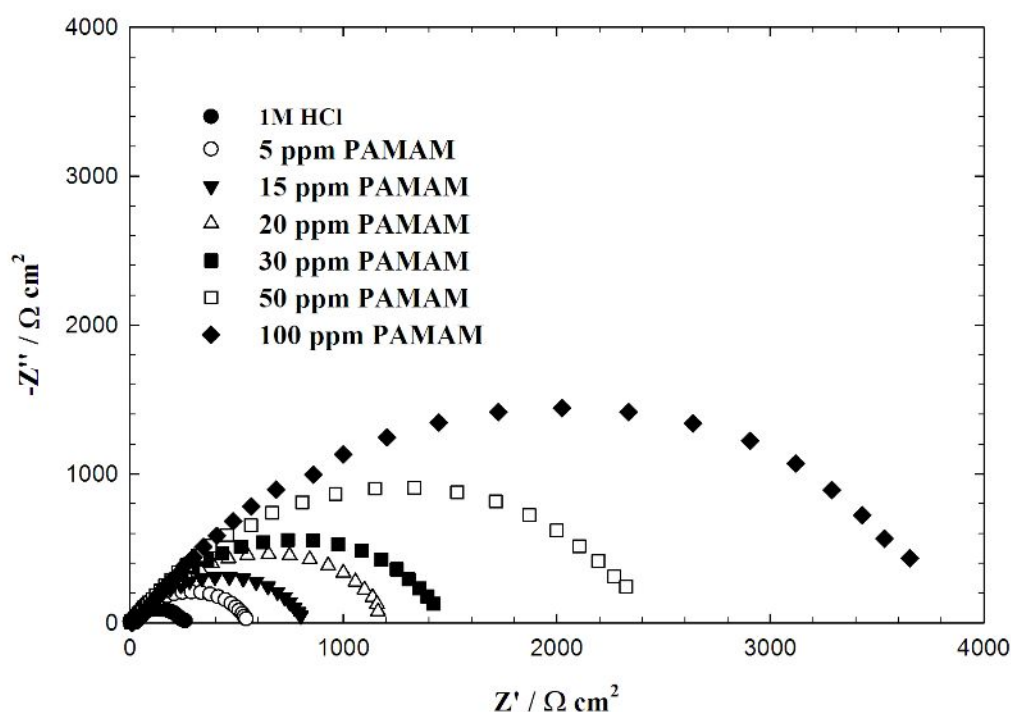


Figure 3: Nyquist plots for Steel 5LX60 in 1.0 M HCl solutions in absence and presence of various concentrations of polyamidoamine dendrimer at 25 ±1 °C

Nyquist plots presented in Figure 3 shows depressed semicircles with the centre under the real axis, such behaviour is characteristic for solid electrodes and often referred to as frequency dispersion and attributed to the roughness and other inhomogeneities of the steel electrode [31-33].

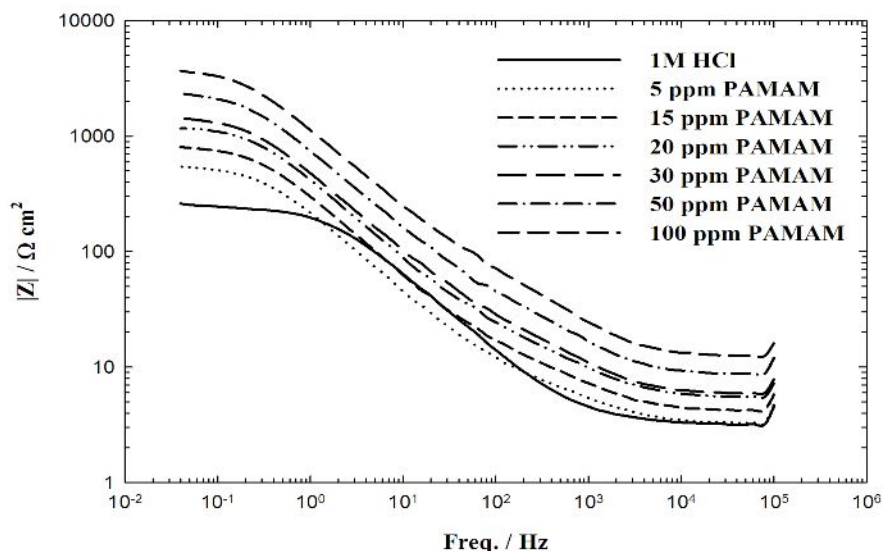


Figure 4: Bode plots for Steel 5LX60 in 1.0 M HCl solutions in absence and presence of various concentrations of Polyamidoamine dendrimer at 25 ± 1 °C

The capacitive loop was related to charge-transfer in corrosion process [34]. The depressed form of the higher frequency loop reflects the surface inhomogeneity of structural or interfacial origin, such as those found in adsorption processes [35].

EIS plots presented in Figure 3-5 are modeled using an equivalent circuit presented in Figure 6, similar to the one proposed by several authors [10, 36, 37].

Parameters derived from equivalent circuit in Figure 6 and inhibition efficiency is given in Tables 2. By increasing the concentration of PAMAM, the values of polarization resistance increase and the CPE values is decreased. The constant phase element (CPE) with their n values $1 > n > 0$ represents double layer capacitors with some pores [38].

This decrease in (CPE) results from a decrease in local dielectric constant and/or an increase in the thickness of the double layer, suggested that PAMAM molecules inhibit the steel corrosion by adsorption at the steel/HCl interface.

The semicircles in Figure 3 are generally associated with the relaxation of electrical double layer capacitors and the diameters of these semicircles can be considered as the charge-transfer resistance ($R_{ct} = R_p$) [39].

Therefore, the inhibition efficiency, E_{IMP} % presented in Tables 2 of PAMAM for the steel electrode can be calculated from the charge-transfer resistance as follows [40]:

$$E_{IMP} \% = \left(1 \epsilon \frac{R_p^o}{R_p}\right) \epsilon 100 \quad (3)$$

where R_p^o and R_p are the polarization resistances calculated from EIS measurements for uninhibited and inhibited solutions, respectively.

The area under $|Z|$ -frequency curves of Bode plots is employed to compare protective performances of PAMAM. Figure 4 shows $|Z|$ -frequency curves obtained for steel electrode in 1.0 M HCl solution in absence and presence of different concentrations of PAMAM. It can be clearly seen from this figure that, the area under the curves is increased with increasing PAMAM concentration[41]. This indicates increasing the protective performance of PAMAM. Phase angle at high frequency is utilized for evaluation of inhibition properties and it is a good criterion in order to determine the protection efficiency. Figure 5 shows phase angle-frequency diagrams of steel/HCl electrode for various PAMAM concentrations. As can be seen from

this figure, phase angles of steel samples at 100 kHz increases with increasing PAMAM concentration. This indicates increasing the corrosion resistance of steel. Consequently, results taken from both change of area under $|Z|$ -frequency curves and change of phase angles at high frequency show similar trend obtained from potentiodynamic polarization curves [41].

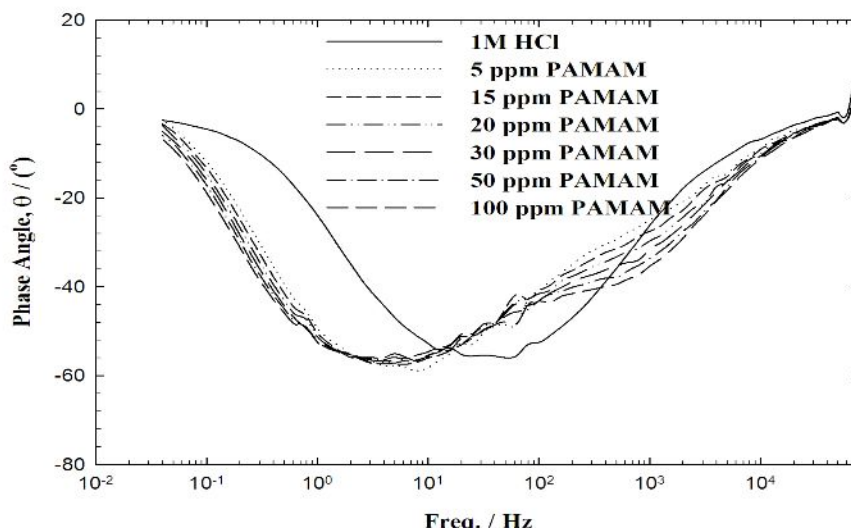


Figure 5: Bode-phase plots for Steel 5LX60 in 1.0 M HCl solutions in absence and presence of various concentrations of polyamidoamine dendrimer at 25 ± 1 °C

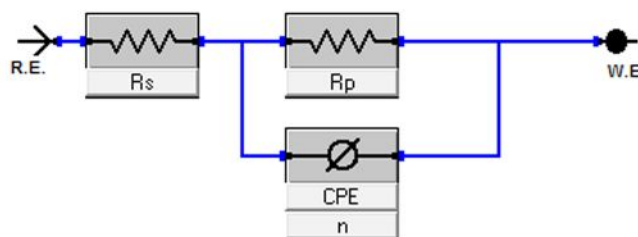


Figure 6: Equivalent circuit model for steel 5LX60 in 1.0 M HCl solutions

Table 2: Electrochemical parameters calculated from EIS measurements on steel 5LX60 electrode in 1M HCl solutions without and with various concentrations of polyamidoamine dendrimer at 25 ± 1 °C by electrochemical impedance spectroscopy.

| Conc. M | R_s $\Omega \cdot \text{cm}^2$ | R_p $\Omega \cdot \text{cm}^2$ | CPE $\Omega^{-1} \text{cm}^2 \text{S}^n$ | n | E_{IMP} % |
|------------|-------------------------------------|-------------------------------------|---|-------|-------------|
| 0.00 | 2.3 | 256 | 43.1 | 0.756 | 0.00 |
| 5 | 3.3 | 546.6 | 33.2 | 0.820 | 53.2 |
| 15 | 2.7 | 805.0 | 29.5 | 0.843 | 68.2 |
| 20 | 2.4 | 1189.0 | 25.1 | 0.786 | 78.4 |
| 30 | 3.1 | 1432.0 | 19.3 | 0.801 | 82.1 |
| 50 | 3.4 | 2337.0 | 15.4 | 0.821 | 89.1 |
| 100 | 4.7 | 3667.0 | 11.2 | 0.810 | 93.0 |

Figure 4 exhibit three different regions. In the high frequency region, the value of $|Z|$ tends to become very small and the corresponding phase angle also falls off very rapidly with increasing frequency. This region is typical of a resistive behaviour and corresponds to solution resistance. In the medium frequency region, a linear relationship exists between $|Z|$ and f and there is a broad maximum in phase angle vs. frequency plot. This region corresponds to the charge transfer at the steel/electrical double layer. In the low frequency segment, the resistive behaviour of the electrode increases and the value of $|Z|$ should remain constant with a further decrease in frequency [42].

In Figure 5, there is only one phase maximum in all these plots and the angle corresponding to the phase maximum is found to be in the range of 52–56°. The total impedance Bode plots indicate that impedance increases with increasing PAMAM concentration. This result infers that with an increase in PAMAM concentration, the suggested film becomes more and more protective.

4.2 Theoretical study

In the current study, the studied dendrimer PAMAM has been simulated as adsorbate on steel surface (111) substrate to find the low energy adsorption sites on the steel surface and to investigate the preferential adsorption of the studied dendrimer. To calculate the adsorption density as well as binding energy of the studied inhibitor, Monte Carlo method has been used. In this computational work, possible adsorption configurations have been identified by carrying out Monte Carlo searches of the configurational space of the steel/ PAMAM inhibitor system as the temperature is slowly decreased. The adsorbate was the studied PAMAM constructed and its energy was optimized using Forcite classical simulation engine [43, 44].

Figure 7 shows the optimized structure of PAMAM obtained using DMol³ module.

Molecular dynamics techniques are applied on a system comprising a PAMAM dendrimer, solvent molecules and steel surface. Each PAMAM molecule is placed on the steel surface, optimized and then run quench molecular dynamics. Each PAMAM is energy optimized before putting it on the steel surface. The Monte Carlo simulation process tries to find the lowest energy for the whole system. The structure of the adsorbate (PAMAM) is minimized until it satisfies certain specified criteria.

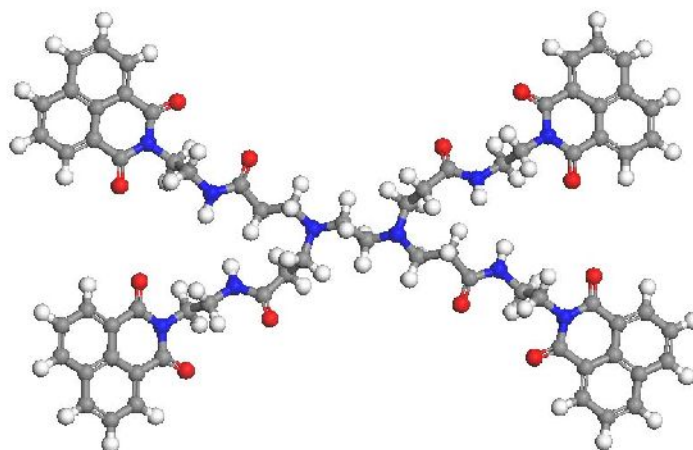


Figure 7: Optimized geometries of PAMAM

The Metropolis Monte Carlo method in Adsorption Locator module provides four step types for a canonical ensemble: conformer, rotation, translation, and re-growth[45].

Figure 8 shows the most suitable PAMAM conformation adsorbed on Fe(111) substrate obtained by adsorption locator module[46-48]. The adsorption density of PAMAM on the Fe(111) substrate has been presented in Figure 9.

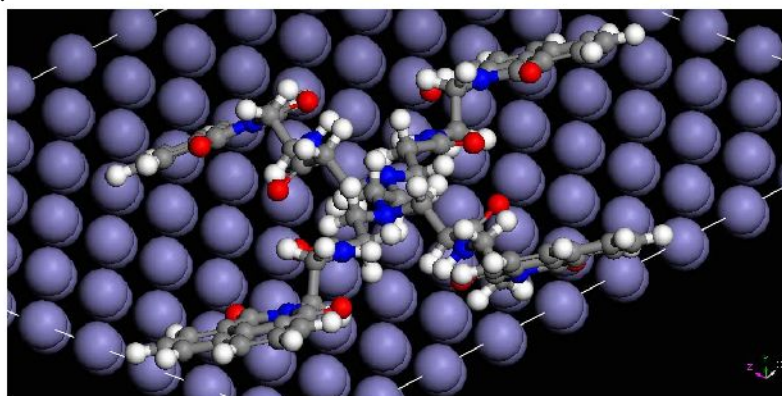


Figure 8: Equilibrium adsorption configurations of PAMAM on Fe (111) surfaces obtained by molecular dynamics simulations

Table 3: Different adsorption structures and the corresponding adsorption energy and binding energies in KJ mol⁻¹

| Structures | Total energy | Adsorption energy | Rigid adsorption energy | Deformation energy | I4 : dE _{ad} /dNi | Binding energies |
|-----------------|--------------|-------------------|-------------------------|--------------------|----------------------------|------------------|
| Fe (1 1 1) - 1 | 4.18E+03 | 3.95E+03 | 2.28E+03 | 1.67E+03 | 3.95E+03 | 1534 |
| Fe (1 1 1) - 2 | 4.20E+03 | 3.97E+03 | 2.33E+03 | 1.65E+03 | 3.97E+03 | 1512 |
| Fe (1 1 1) - 3 | 4.20E+03 | 3.97E+03 | 2.32E+03 | 1.65E+03 | 3.97E+03 | 1423 |
| Fe (1 1 1) - 4 | 4.25E+03 | 4.02E+03 | 2.27E+03 | 1.75E+03 | 4.02E+03 | 1412 |
| Fe (1 1 1) - 5 | 4.25E+03 | 4.02E+03 | 2.17E+03 | 1.85E+03 | 4.02E+03 | 1356 |
| Fe (1 1 1) - 6 | 4.27E+03 | 4.03E+03 | 2.21E+03 | 1.83E+03 | 4.03E+03 | 1321 |
| Fe (1 1 1) - 7 | 4.27E+03 | 4.04E+03 | 2.29E+03 | 1.75E+03 | 4.04E+03 | 1311 |
| Fe (1 1 1) - 8 | 4.27E+03 | 4.04E+03 | 2.30E+03 | 1.74E+03 | 4.04E+03 | 1306 |
| Fe (1 1 1) - 9 | 4.28E+03 | 4.05E+03 | 2.19E+03 | 1.85E+03 | 4.05E+03 | 1300 |
| Fe (1 1 1) - 10 | 4.28E+03 | 4.05E+03 | 2.26E+03 | 1.79E+03 | 4.05E+03 | 1301 |

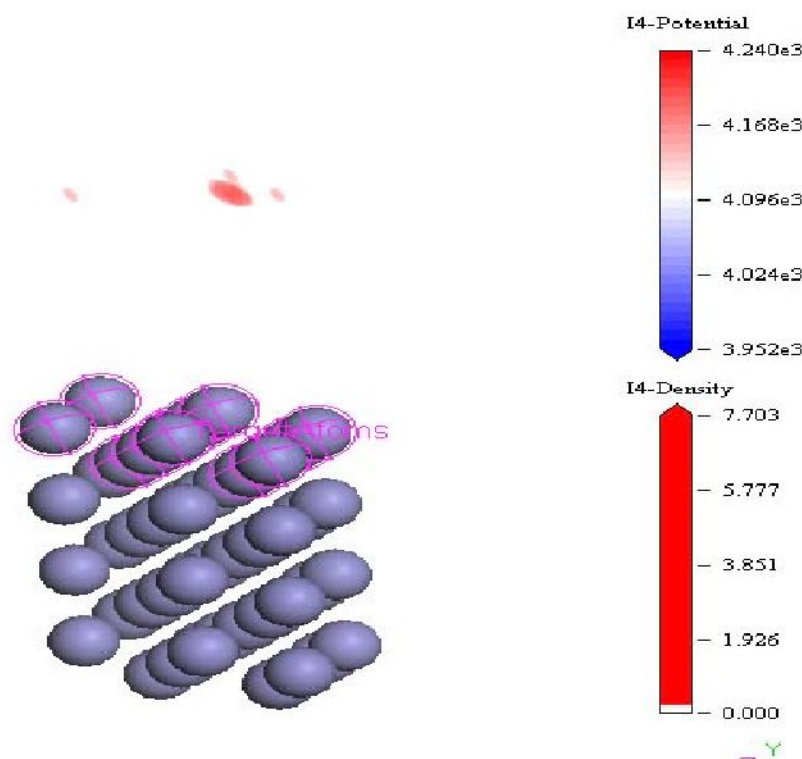


Figure 9: Adsorption density field of PAMAM on Fe (111) substrate.

As can be seen from Figures 8-9 that the dendrimer molecule PAMAM shows good ability to adsorb on Fe (111) surface. Also, it has high binding energy to steel surface as seen in Table 3.

Figure 10 shows the adsorption energy distribution of PAMAM on steel surface. The descriptors calculated by Monte Carlo simulation are presented in Table 3. These descriptors existing in Table 3 include total energy, in kJ per mole, of the substrate–adsorbate configuration. Total energy in Table 3 is defined as the sum of the energies of the adsorbate components, the rigid adsorption energy and the deformation energy. In this study, the substrate energy (iron surface) is taken as zero. In addition, adsorption energy in kJ per mole, reports energy released (or required) when the relaxed adsorbate components (PAMAM in H₂O) are adsorbed on the substrate. The adsorption energy is defined as the sum of the rigid adsorption energy and the deformation energy for the adsorbate components.

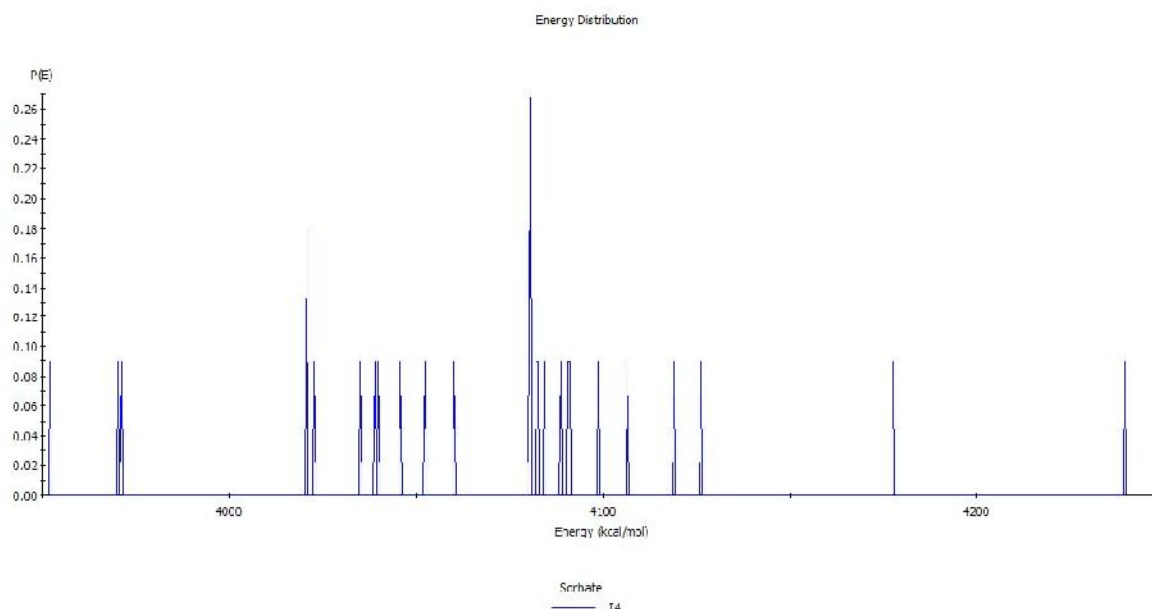


Figure 10: Energy distribution of PAMAM on Fe (111) surfaces obtained by molecular dynamics simulations

The rigid adsorption energy reports the energy, in kJ mol^{-1} , released (or required) when the unrelaxed adsorbate components (i.e., before the geometry optimization step) are adsorbed on the substrate. The deformation energy reports the energy, in kJ per mole, released when the adsorbed adsorbate components are relaxed on the substrate surface. Table 3 shows also that (dE_{ads}/dN_i) , which reports the energy, in kJ per mole, of substrate–adsorbate configurations where one of the adsorbate components has been removed.

Conclusion

The following conclusions can be drawn from the study:

The results showed that PAMAM dendrimer has excellent inhibition efficiency for the corrosion of steel in 1.0 M HCl. The inhibition efficiency increases in as the concentration of PAMAM increases.

The potentiodynamic polarization curves indicated that PAMAM acts as cathodic-type inhibitor.

The impedance results indicate that the value of polarization resistance increased and CPE decreased by increasing PAMAM concentration. This result can be attributed to the increase of thickness of electrical double layer.

Acknowledgements—Authors gratefully acknowledge Taif University (Project # 1-345-2540) for the financial assistance and facilitation of our study.

References

1. El Azhar M., Traisnel M., Mernari B., Gengembre L., Bentiss F., Lagrenée M., *Appl. Surf. Sci.*, 185 (2002) 197.
2. Karthikaiselvi R., Subhashini S., Rajalakshmi R., *Arab. J. Chem.*, 5 (2012) 517.
3. Gao B., Zhang X., Sheng Y., *Mater. Chem. Phys.*, 108 (2008) 375.
4. Khaled K. F., Abdelshafi N. S., *Int. J. Electrochem. Sci.*, 8 (2013) 1409.
5. Khaled K. F., El-Sherik A. M., *Int. J. Electrochem. Sci.*, 8 (2013) 10022.
6. Khaled K. F., El-Sherik A. M., *Int. J. Electrochem. Sci.*, 8 (2013) 9918.
7. Sultan, A.A., Ateeq, A.A., Khaled, N.I., Taher, M.K., Khalaf, M.N., *J. Mater. Environ. Sci.*, 5 (2014) 498.
8. Khaled K., Abdel-Shafi N., Al-Mobarak N., *Int. J. Electrochem. Sci.*, 7 (2012) 1027.
9. Rajeev P., Surendranathan A.O., Murthy Ch. S.N., John Berchmans L., *J. Mater. Environ. Sci.*, 5 (2014) 440.
10. Khaled K. F., Abdel-Rehim S. S., Sakr G. B., *Arab. J. Chem.*, 5 (2012) 213.
11. Loera-Serna S., Oliver-Tolentino M. A., De Lourdes López-Núñez M., Santana-Cruz A., Guzmán-Vargas A., Cabrera-Sierra R., Beltrán H. I., Flores J., *J. Alloys Compd.*, 540 (2012) 113.
12. Dar M. A., *Ind. Lub.Tribol.*, 63 (2011) 227.
13. Mishra A., Godhani D. R., Sanghani A., *J. Chem. Pharm. Res.*, 3 (2011) 388.
14. Tsangaraki-Kaplanoglou I., Kanta A., Theohari S., Ninni V., *Anti-Corros Method Mater.*, 57 (2010) 6.
15. Xu J., Zhou C., Chen Z., Wang Y., Jiang S., *J. Alloys Compd.*, 496 (2010) 429.
16. Li X., Deng S., Fu H., Li T., Mu G., *Anti-Corros Method M.*, 56 (2009) 232.
17. Tuken T., Demir F., Kicir N., Sigircik G., Erbil M., *Corros. Sci.*, 59 (2012) 110.

18. Zunita M., Wahyuningrum D., Buchari, Bundjali B., *Int. J. Electrochem. Sci.*, 7 (2012) 3274.
19. Amin M. A., Shokry H., Mabrouk E. M., *Corrosion*, 68 (2012) 699.
20. Akalezi C. O., Ogukwe C. E., Enenebaku C. K., Oguzie E. E., *Environ.Poll.*, 1 (2012) 45.
21. Udhayakala P., Rajendiran T. V., Gunasekaran S., *J. Chem. Bio. Phy. Sci. (JCBPS)*, 2 (2012) 1151.
22. Qian B., Wang J., Zheng M., Hou B., *Corros. Sci.*, 75 (2013) 184.
23. Peleshanko S., Tsukruk V. V., *Prog.Poly. Sci.*, 33 (2008) 523.
24. Kiehl A., Brendel H., *Macro. Symp.*, 187 (2002) 109.
25. Shahba R.M.A., Ahmed A.S.I., El-Shenawy A. E.-S., Ghannem W.A., Tantawy S.M., *Inter. J. Chem.*, 4 (2012) 30.
26. Prabhu R. A., Venkatesha T. V., Praveen B. M., *ISRN Metallurgy*, (2012).
27. Benmessaoud M., Es-salah K., Kabouri A., Hajjaji N., Takenouti H., Srhiri A., *Mater. Sci. Appl.*, 2 (2011) 276.
28. Hermann B. A., Hubler U., Jess P., Lang H. P., Güntherodt H. J., Greiveldinger G., Rheiner P. B., Murer P., Sifferlen T., Seebach D., *Surf. Interface Anal.*, 27 (1999) 507.
29. Demadis K. D., *J. Chem. Technol. Biotechnol.*, 80 (2005) 630.
30. Refat M. S., El-Deen I. M., Grabchev I., Anwer Z. M., El-Ghol S., *Spectrochim. Acta Mol. Biomol. Spectros.*, 72 (2009) 772.
31. Ma H., Chen S., Niu L., Zhao S., Li S., Li D., *J. Appl. Electrochem.*, 32 (2002) 65.
32. Khaled K. F., Al-Mobarak N. A., *Int. J. Electrochem. Sci.*, 7 (2012) 1045.
33. Zarrouk A., Hammouti B., Zarrok H., Bouachrine M., Khaled K.F., Al-Deyab S.S., *Int. J. Electrochem. Sci.*, 7 (2012) 89.
34. Ashassi-Sorkhabi H., Ghalebsaz-Jeddi N., Hashemadef F., Jahani H., *Electrochim. Acta*, 51 (2006) 3848.
35. Gonçalves R. S., Azambuja D. S., Serpa Lucho A. M., *Corros. Sci.*, 44 (2002) 467.
36. Khaled K. F., *J. Electrochem. Soc.* 158 (2011) S28.
37. Han L., Song S., *Corros. Sci.*, 50 (2008) 1551.
38. Sherif E. M., Park S. M., *Electrochim. Acta*, 51 (2006) 1313.
39. Khaled K. F., Abdel-Shafi N. S., Al-Mobarak N. A., *Int. J. Electrochem. Sci.*, 7 (2012) 1027.
40. Khaled K. F., Abdel-Rehim S. S., Sakr G. B., *Arab. J. Chem.*, 5 (2012) 213.
41. Çakmakci I., Duran B., Bereket G., *Prog. Org. Coat.*, 76 (2013) 70.
42. Appa Rao B. V., Chaitanya Kumar K., *Arab. J. Chem.* <http://dx.doi.org/10.1016/j.arabjc.2013.07.060>
43. Khaled K. F., Abdel-Shafi N. S., *Int. J. Electrochem. Sci.*, 6 (2011) 4077.
44. Ermer O., Calculation of molecular properties using force fields. Applications in organic chemistry, in: Bonding forces, vol. 27, Springer Berlin Heidelberg, 1976, pp. 161-211.
45. Guedes Soares C., Garbatov Y., Zayed A., Wang G., *Corros. Sci.*, 50 (2008) 3095.
46. Tamura H., *Corros. Sci.*, 50 (2008) 1872.
47. Tan Y., *Corros. Sci.*, 53 (2011) 1845.
48. Gudze M. T., Melchers R. E., *Corros. Sci.*, 50 (2008) 3296.

(2014); <http://www.jmaterenvironsci.com/>